Available online at www.sciencedirect.com

SCIENCE DIRECT®

Journal of Photochemistry and Photobiology A: Chemistry 178 (2006) 8–15

Journal of Photochemistry and Photobiology A:Chemistry

www.elsevier.com/locate/jphotochem

Visible light photoelectrochemical and water-photoelectrolysis properties of titania nanotube arrays

Maggie Paulose, Gopal K. Mor, Oomman K. Varghese, Karthik Shankar, Craig A. Grimes*

Department of Electrical Engineering, Department of Materials Science and Engineering, and The Materials Research Institute,
The Pennsylvania State University, 217 MRL, University Park, PA 16802, USA

Received 11 April 2005; received in revised form 14 June 2005; accepted 14 June 2005
Available online 20 July 2005

Abstract

We examine the visible light water-photoelectrolysis and photoelectrochemical properties of highly ordered titania nanotube arrays as a function of nanotube crystallinity, length (up to 6.4 μm), and pore size. Most noteworthy of our results, under visible light AM 1.5 illumination (100 mW/cm^2) the titania nanotube array photoanodes (1 cm^2 area), pore size 110 nm, wall thickness 20 nm, and length 6 μm, generate hydrogen by water photoelectrolysis at a rate of 175 μL/h, with a photoconversion efficiency of 0.6%. The energy–time normalized hydrogen evolution rate is 1.75 mL/h W. The oxygen bubbles evolving from the nanotube array photoanode do not remain on the sample, hence the output remains stable with time irrespective of the duration of hydrogen production.

Keywords: Hydrogen; Photolysis; Photoelectrolysis; Titania; Nanotube; Nanotube array

1. Introduction

Using solar energy to split water generating hydrogen and oxygen offers a clean, portable source of energy the supply of which is as durable as our sunlight [1]. Fujishima and Honda reported hydrogen generation by water photoelectrolysis using n-type TiO_2 in 1972 [2]; since then considerable efforts have focused on development and application of photoelectrochemical cells using numerous material platforms in a variety of material architectures [3–5]. Oxide materials are attractive because of their ability to withstand photocorrosion, wide-spread availability, and affordability; however, without band gap engineering most of the stable oxides are photochemically active only in ultraviolet (UV) light [3–7], the energy of which makes up only a small fraction of the solar spectrum. The development of an oxide material system realistically useful for water-photoelectrolysis faces two fundamental challenges. One challenge, on which there have been many studies [3–6] is shifting of the materials absorption spectra from UV into the visible light region where the majority of the solar spectrum energy is resident. An equally important challenge, which our present work is concerned with, is that a useful system for water-photoelectrolysis requires a material architecture able to achieve efficient charge transfer so the photo-generated electrons and holes perform significant work splitting water, rather than simply recombining. Several micron-thick porous nanoparticulate films, comprised of a three dimensional network of interconnected 15–20 nm nanoparticles, have so far been identified as the most suitable oxide material architecture for photochemical processes [7–9]. However, while the large surface area of the porous nanoparticulate films enables efficient light harvesting and the electron–hole pairs generated by optical absorption are separated kinetically [10], system efficiency is limited by the poor electron transport through the network [11]. Consequently there has been considerable interest in ordered nanostructures such as arrays of nanowires [12], nanorods [13,14], template formed and thin-film nanotube ‘mats’ [15–17] for potentially enhancing electron percolation pathways, light conversion, as well as improved ion diffusion at the semiconductor–electrolyte interface. Yet to

---

* Corresponding author. Tel.: +1 8148659142; fax: +1 8148656780.
E-mail address: cgrimes@engr.psu.edu (C.A. Grimes).

1010-6030/$ – see front matter © 2005 Elsevier B.V. All rights reserved.
doi:10.1016/j.jphotochem.2005.06.013

date such structures have shown no property improvements beyond those of the nanoparticulate films [18].

Our approach to achieving an optimal material architecture for water-photoelectrolysis uses a simple anodization technique to fabricate titania with a unique nanoarchitecture consisting of vertically oriented, immobilized, highly ordered high-aspect ratio nanotubes. We earlier reported the synthesis [19–22], and application of short, up to about 500 nm long, titania nanotube arrays to hydrogen gas sensing and self-cleaning surfaces [23]. We note the hydrogen sensitivity of the material, about seven orders of magnitude (1,000,000,000%) change in the electrical resistance at 23 °C in response to 1000 ppm hydrogen, appears to be the largest known sensitivity of any material at any temperature to any gas [24]. Our earlier studies on the fabrication of titania nanotube arrays, and properties thereof, utilized a low pH anodization bath that resulted in fabrication of nanotube arrays only several hundred nm in length. Recently, we successfully modified the anodization conditions to obtain longer nanotube arrays, up to about 4.4 μm [25]. As we report herein, we have further improved the anodization conditions increasing the length of the nanotube arrays to over 6.4 μm (pore diameter 110 nm and wall thickness ∼ 20 nm). Since the photoelectrochemical and gas sensing properties of the nanotubes are dependent upon their length the ability to fabricate significantly longer nanotube arrays is an important advance. The significantly longer nanotube arrays provide a greater surface area for photoelectrochemical interaction, while the tubular structure makes the regions both inside and outside the tubes (inter-tubular region) easily accessible to the redox couples in the electrolyte. The large surface area of the nanotubular structure and the precise tuning of pore sizes, wall-thickness, and nanotube length are among the many desirable properties of this architecture. In an earlier report [26] we discussed the water-photoelectrolysis properties of short nanotube arrays, up to approximately 225 nm in length, under UV illumination as a function of nanotube-wall thickness. Upon 95 mW/cm^2 320–400 nm illumination a nanotube array of 22 nm pore-diameter, 34 nm wall thickness, and 224 nm length generated hydrogen by water photoelectrolysis with an overall conversion efficiency of 6.8% [26].

The present paper describes the photoelectrochemical properties of titania nanotube arrays under visible light (AM 1.5) illumination as a function of length 1.8–6.4 μm, nanotube pore diameter 22–180 nm, and crystallization temperatures. Our results indicate that the nanotube array films are an excellent material architecture for water photoelectrolysis, with a hydrogen generation rate and photoconversion efficiency much higher than other oxide material architectures studied so far [3,4,27,28].

2. Experimental

Fig. 1 illustrates the arrangement used for anodizing the Ti films. The anodization of titanium is accompanied with the chemical dissolution of titanium oxide due to the formation of TiF_6^{2-} [21]. The ultimate concentration of F^- and HF are determined by the solution pH. The high rate of chemical dissolution of the oxide in hydrofluoric acid containing electrolytes of low pH limits the nanotube length to a few hundred nanometers. In contrast, use of potassium fluoride (KF) or sodium fluoride (NaF) electrolytes slows the oxide dissolution rate, enabling nanotube arrays several microns in length [25]. Relatively longer nanotube arrays are grown using anodic oxidation of titanium foils (99.8% pure) in an electrolyte containing potassium fluoride (KF; 0.1 M), sodium hydrogen sulfate (1 M), trisodium citrate (0.2 M) and sodium hydroxide (Aldrich, Milwaukee, WI). Fig. 2 illustrates the change in anodization current with time, under constant voltage, as a starting Ti foil electrochemically etches. In this case the Ti foil sample size is 1 cm^2, 25 V potential, pH 4.5, with the sample immersed in a KF electrolyte containing sodium hydrogen sulfate, trisodium citrate and sodium hydroxide; the resulting nanotubes have a length of approximately 4.4 μm. For all electrolytes the resulting as-prepared samples are amorphous; for crystallization samples are annealed at temperatures ranging from 250 to 700 °C in oxygen ambient for 6 h employing a heating/cooling rate of 1 °C/min.

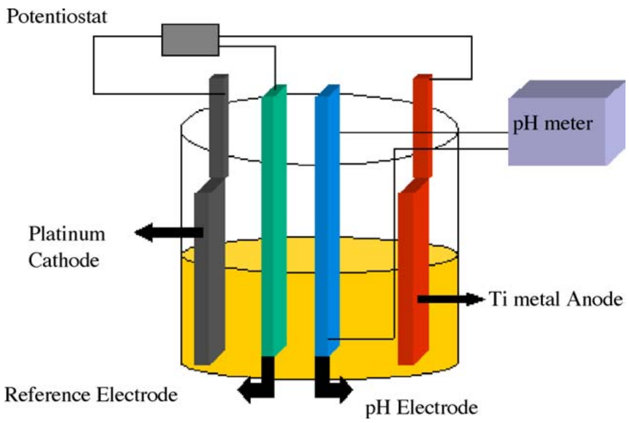

Fig. 1. Illustrative drawing of a three-electrode electrochemical cell in which the Ti samples are anodized as a function of voltage, pH and electrolyte composition.

Fig. 3 shows a FE-SEM (JEOL, Tokyo) cross-sectional image of a nanotube array grown over a 17 h anodization

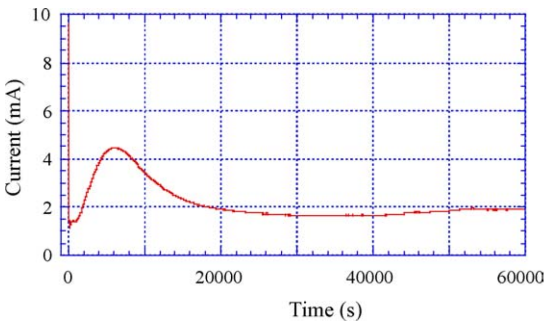

Fig. 2. Illustrative plot of the potentiostatic anodization of Ti metal in a KF electrolyte.

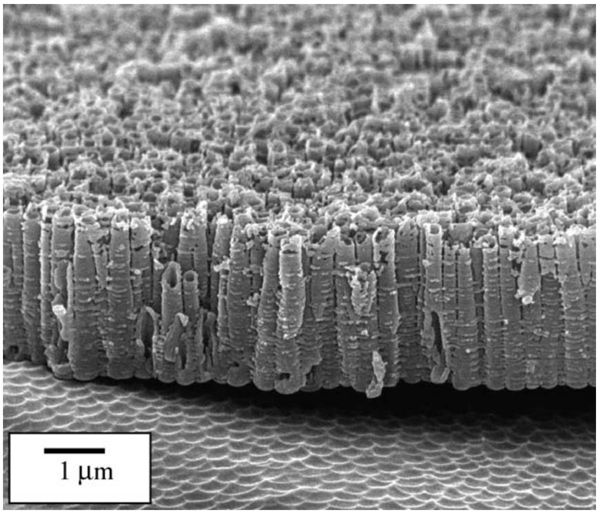

Fig. 3. FESEM cross-sectional image of 2.8 μm long TiO_2 nanotube array prepared by anodic oxidation of a titanium foil in an electrolyte containing potassium fluoride (KF; 0.1 M), sodium hydrogen sulfate (1 M), trisodium citrate (0.2 M) and sodium hydroxide. The nanotubes were formed in an electrolyte of pH 4.0 over a 17 h period at an anodization potential of 25 V. The sample was intentionally cracked for viewing.

period, in a KF electrolyte at pH 4.0 using a potential of 25 V. The tubes grow perpendicular to the substrate forming an array. These tubes have an average length of ≈2.8 μm, inner diameter 110 nm and wall thickness 20 nm. With the same electrolyte composition, and using the same anodization period of 17 h, tubes grown at pH values 3, 4, 4.5 and 5.0 have, respectively, average lengths of 1.8, 2.8, 4.4, and 6.0 μm with all other dimensions the same as the 2.8 μm tubes. The tubes retain their structure on annealing to temperatures as high as 675 °C in oxygen, with higher temperatures oxidizing the underlying titanium foil leading to destruction of the nanotube array. Fig. 4 shows the surface topology of the nanotube array at different levels of magnification.

Fig. 5a is a TEM (Model 420T, Philips) image of a single nanotube grown from a sample prepared at pH 5.0 and annealed at 600 °C. The diffraction pattern, shown in Fig. 5b, from a group of tubes, indicates the presence of anatase phase in the walls; rutile phase was not found in the tube walls. The glancing angle (2°) X-ray diffraction patterns (GAXRD, Scintag Pad V, Cupertino, CA) of nanotubes prepared at pH 5.0 and annealed at temperatures from 250 to 700 °C are shown in Fig. 6. The nanotubes annealed at 330 °C showed traces of anatase crystallites. The rutile phase started appearing at 530 °C, with the rutile phase dominating in samples annealed at 700 °C. The rutile crystallites originate in the oxide layer (formed by the oxidation of titanium metal) underneath the nanotubes at high temperatures through nucleation and growth as well as phase transformation of anatase crystallites existing in the region. The anatase crystallites at the tube walls do not undergo transformation to rutile phase due to the constraints imposed by the walls [20,25,29]. With increasing annealing temperature anatase crystal growth occurs along the length of the tubes consuming the smaller crystallites and amorphous regions [30], with the crystallite width limited by the wall thickness. Consequently a tube annealed at temperatures near 600 °C can be viewed as a hollow nano-column made of stacked anatase crystallites with a rutile base.

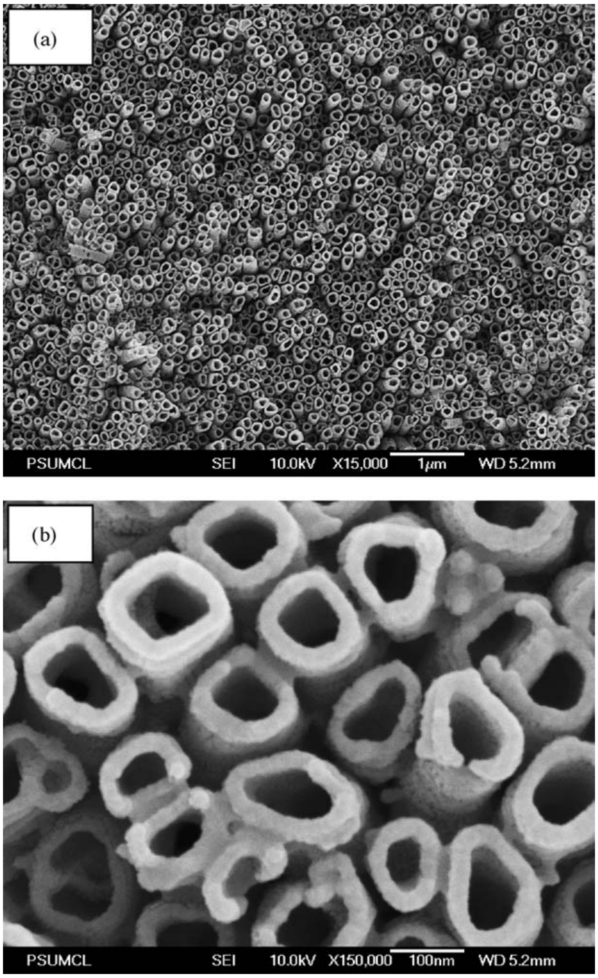

Fig. 4. FESEM images showing top view of an illustrative nanotube array at different levels of magnification.

3. Results and discussion

The electrochemical properties of the samples were characterized using a three electrode photochemical cell with nanotube arrays on titanium foil as the working photoelectrode, saturated Ag/AgCl reference electrode, and platinum foil counter electrode. 1 M KOH solution was used as the electrolyte. A scanning potentiostat (CH Instruments, model CHI 600B) was used to scan the potential at a rate of 20 mV/s and measure the current. The samples were mounted on a glass base and the electrical contacts were taken from the titanium substrate using copper leads and silver epoxy after removing the oxide layer at the titanium surface. All the regions except a 1 cm^2 sample where covered using an insulating epoxy. A Spectra Physics Simulator with an illumination intensity of

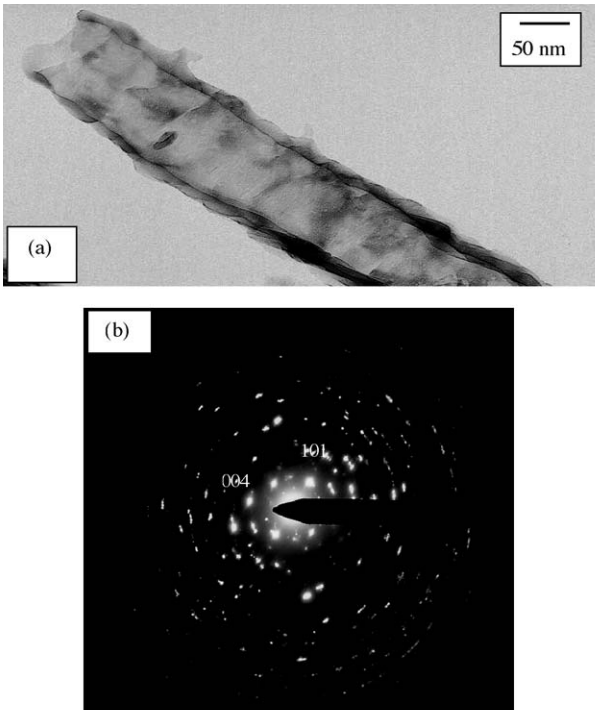

Fig. 5. (a) TEM image of a single nanotube from a sample prepared at pH 5.0 and annealed at 600 °C and (b) corresponding diffraction pattern.

1 sun (AM 1.5, 100 mW/cm^2) with a filter to remove light of wavelength below 400 nm was used as the light source. A PHIR CE power meter was used to calibrate the input power before and after the photoelectrochemical measurements.

3.1. Effect of nanotube array length

For a given KF or NaF electrolyte, the length of the resulting nanotube array is controlled by varying the electrolyte pH by addition of sodium hydroxide. So long as the pH remains acidic it appears that higher pH values result in longer nanotubes given longer anodization periods. For example, using KF (25 V potential, 17 h anodization) tubes grown at pH values 3, 4, 4.5 and 5.0 have, respectively, average lengths of 1.8, 2.8, 4.4, and 6.0 μm. The pH of the electrolyte remains constant during the anodization process.

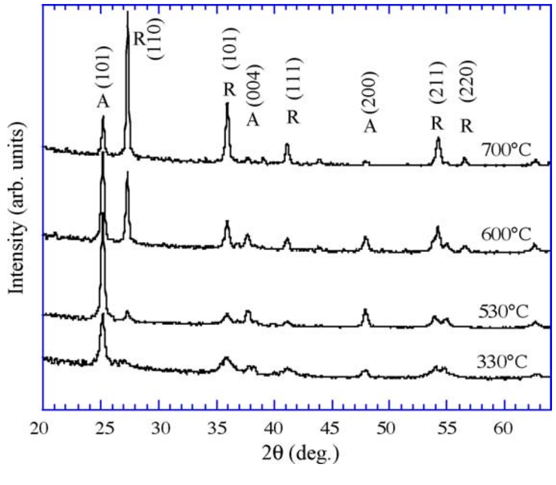

Fig. 6. Glancing angle X-ray diffraction (2°) patterns of a 6 μm long nanotube array as a function of annealing temperatures (oxygen ambient).

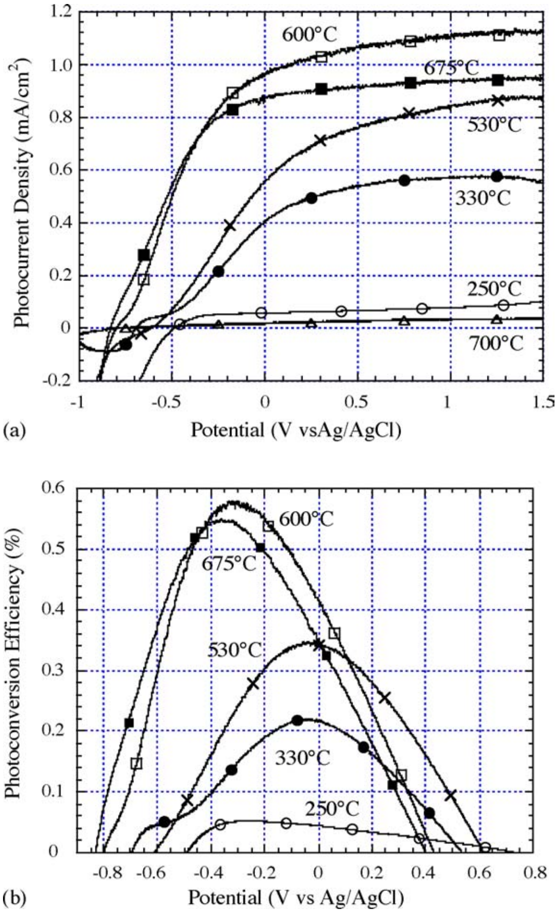

Fig. 7. (a) Visible light (AM 1.5) photocurrent generated from 6 μm long nanotube arrays with respect to annealing temperature and (b) the corresponding photoconversion efficiencies.

Fig. 7a shows the *I*–*V* characteristics under visible light illumination of 6 μm long nanotube arrays annealed at different temperatures; the dark current in all cases is approximately 10^{-7} to 10^{-6} A. The photocurrent increases with increasing annealing temperature to approximately 620 °C, after which it reduces with samples annealed at 700 °C showing a low photocurrent ($\sim 10^{-4}$ A). The corresponding light energy to chemical energy conversion (photoconversion) efficiencies are shown in Fig. 7b. The photoconversion efficiency η was calculated as follows [31]:

$$\begin{aligned}\eta(\%) &= [(\text{total power output} \\ &\qquad - \text{electrical power output})/\text{light power input}] \times 100 \\ &= j_{\mathrm{p}}[(E^0_{\mathrm{rev}} - |E_{\mathrm{app}}|)/I_0] \times 100\end{aligned}$$

where j_{p} is the photocurrent density (mA/cm^2), $j_{\mathrm{p}}E^0_{\mathrm{rev}}$ the total power output, $j_{\mathrm{p}}|E_{\mathrm{app}}|$ the electrical power input and

I_0 is the power density of incident light (mW/cm^2). $E^0_{\rm rev}$ is the standard reversible potential which is 1.23 V/NHE and the applied potential $E_{\rm app} = E_{\rm meas} - E_{\rm aoc}$, where $E_{\rm meas}$ is the electrode potential (versus Ag/AgCl) of the working electrode at which photocurrent was measured under illumination and $E_{\rm aoc}$ is the electrode potential (versus Ag/AgCl) of the same working electrode at open circuit conditions under same illumination and in the same electrolyte [32,33].

The highest visible spectrum efficiency (see Fig. 7b) of about 0.6% was obtained for samples annealed in the range 580–620 °C. The increase in photocurrent and efficiency are due to the increased crystallinity of the nanotube-walls, with the reduction of the amorphous regions and grain boundaries in turn reducing the number of charge carrier recombination centers. However, at temperatures above ≈620 °C the densification of the bottom part of the nanotubes starts isolating the undestroyed nanotubes from the metal electrode reducing the number of charge carriers reaching the electrode. The photoconversion efficiency of the 700 °C annealed sample is negligible, approximately 0.025%. Fig. 8 shows the effect of nanotube array length on the photoresponse, with all samples annealed at 530 °C; both photocurrent magnitude (Fig. 8a) and photoconversion efficiency (Fig. 8b) are seen to increase with length.

Fig. 9 is an illustrative drawing of the experimental setup for the water-photoelectrolysis measurements with the nanotube arrays used as the photoanodes from which oxygen is evolved. We note that the oxygen bubbles evolving from the nanotube array photoanode do not remain on the on the sample, hence the output remains stable with time irrespective of the duration of hydrogen production. Confirmation of the water-splitting reaction is obtained by the 2:1 ratio of evolved hydrogen to oxygen (GC; SRI, model 8610C). The nanotube array photoanodes were held at constant voltage bias, determined by the peak position in the photoconversion efficiency curve with respect to the Ag/AgCl electrode. The effect of nanotube array length on the hydrogen evolution rate under AM 1.5 illumination is given in Fig. 10, with all samples in this experiment annealed at 530 °C. Fig. 11 shows the hydrogen generated as a function of time (mL) using a 6 μm nanotube array annealed at 600 °C. The corresponding hydrogen evolution rate is 175 μL/h (from 1 cm^2 electrode area for AM 1.5 100 mW/cm^2 illumination) or, on a Watt-

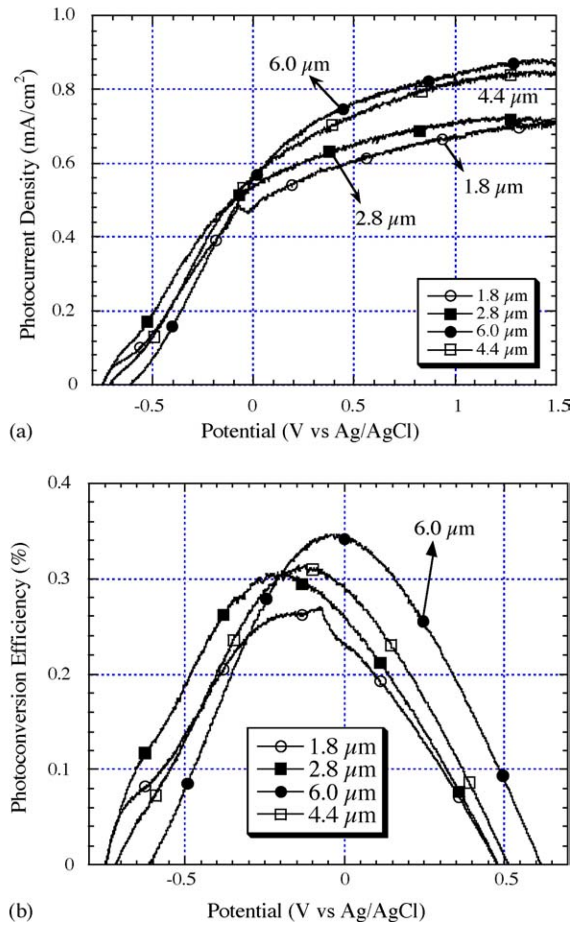

Fig. 8. (a) Visible light (AM 1.5) photocurrent generated from nanotube arrays of different lengths annealed at 530 °C and (b) the corresponding photoconversion efficiencies.

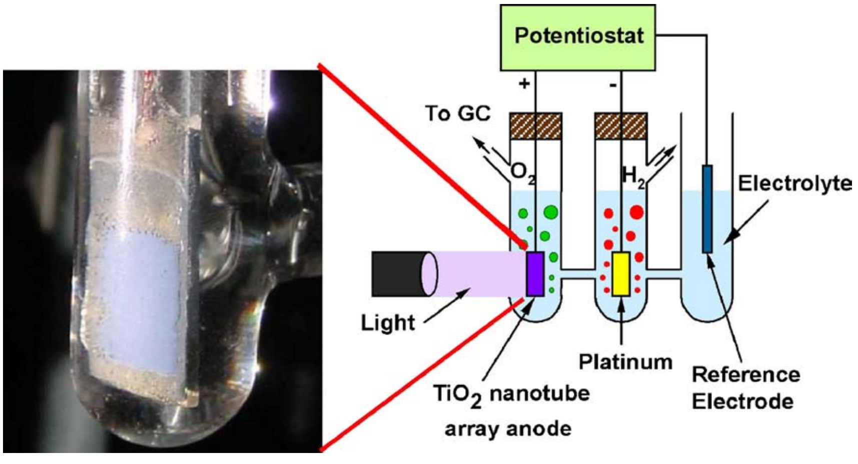

Fig. 9. Illustrative drawing of the experimental set-up for hydrogen generation by water photoelectrolysis.

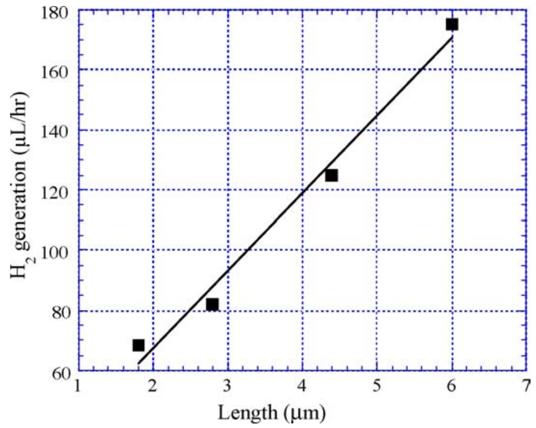

Fig. 10. The rate of hydrogen generation from crystallized nanotube arrays of different lengths annealed at 530 °C. An electrode area of 1 cm^2 was exposed to 100 mW/cm^2 AM 1.5 illumination in all cases.

normalized basis, 1.75 mL/W h. No degradation in sample properties has been observed with UV/visible light exposure over the course of several months.

3.2. *Effect of nanotube array pore size*

Nanotube pore size is predominately determined by the anodization voltage, but also by the electrolyte composition and pH. Hence it is difficult to uniquely determine the role nanotube pore size plays in determining the photoelectrochemical properties, since more than one geometrical feature is changing per given fabrication parameter. For a KF electrolyte, pH 3, we have made nanotube samples at 10 V (30 nm pore, 0.7 μm length), 15 V (50 nm pore, 1.2 μm length), and 25 V (110 nm pore, 1.8 μm length). Hence while pore size is varying by approximately 4×, length is varying by 2.5×. Fig. 12a shows the resulting photocurrents, for 530 °C annealed samples, as a function of applied anodization potential, with the corresponding photoconversion efficiencies seen in Fig. 12b. With reference to Fig. 12, we note that (unpublished) finite difference time domain (FDTD) simulations by the authors show nanotube arrays of small pore diameters, ≈20 nm, reflect significantly larger amounts of incident energy from their surfaces than their larger pore counterparts due to a higher average dielectric constant.

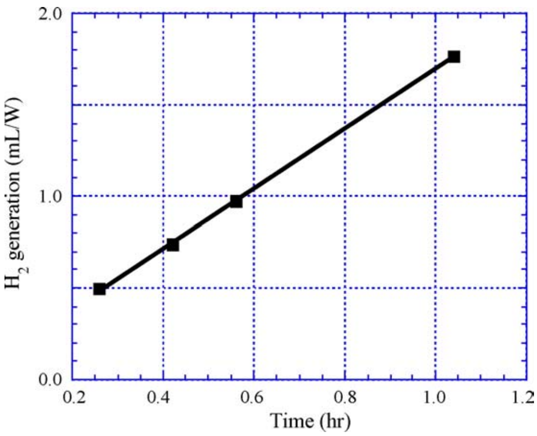

Fig. 11. The amount of hydrogen generated as a function of time using a 6 μm nanotube array annealed at 600 °C; the Watt-normalized generation rate corresponds to 1.75 mL/W h. An electrode area of 1 cm^2 was exposed to 100 mW/cm^2 AM 1.5 illumination.

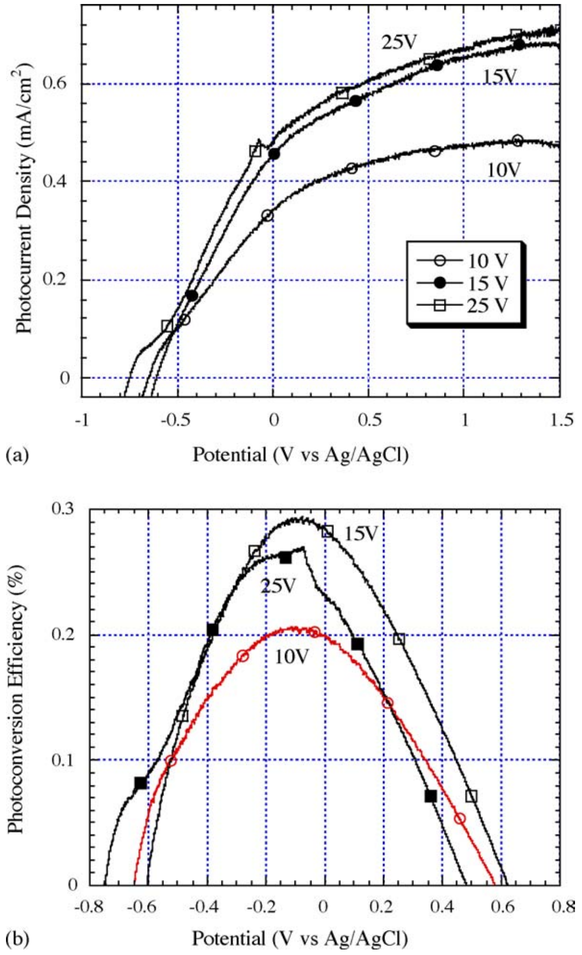

Fig. 12. Preliminary investigation into the role nanotube pore size plays in determining photoelectrochemical properties. The nanotube array photoanodes were made using a KF electrolyte, pH 3, at 10 V (30 nm pore, length 0.7 μm), 15 V (50 nm pore, length 1.2 μm), and 25 V (110 nm pore, length 1.8 μm). (a) Resulting photocurrent and (b) corresponding photoconversion efficiencies.

The highly ordered titania nanotube array structure enables the conductive electrolyte to permeate the entire internal and external surfaces, hence there is a constant electrostatic potential along the length of the tubes (no RC ladder effect). Therefore, long-range electron transport is dominated by diffusion rather than drift [34]. The nanotube array architecture, with a wall thickness of 20 nm, ensures that the holes are never generated far from the semiconductor–electrolyte interface. Furthermore, since the wall thickness is much less than the minority carrier diffusion length $L_p \approx 100$ nm in TiO_2 [35], charge carrier separation takes place efficiently. The increased crystallinity of the samples annealed at elevated temperatures reduces the number of grain boundaries, improves connectivity between grains and eliminates any amorphous regions that provide defects that can act as carrier recombination centers.

The width of the anatase crystallites in the walls is restricted by the wall thickness, approximately 20 nm. The potential drop within the wall can be represented as

$$\Delta\phi_0 = kTr_0^2/6eL_\mathrm{D}^2$$

where r_0 is half the width of the wall, T the temperature, and L_D is the Debye length given by

$$L_\mathrm{D} = [\varepsilon_0\varepsilon kT/2e^2N_\mathrm{D}]^{1/2}$$

where N_D is the number of ionized donors per cm^3 [36]. This potential drop across the wall thickness may not be enough to separate the photogenerated electrons and holes, however, due to the nanoscale dimensions of the walls the holes can reach the electrolyte surface through diffusion, which takes place on a scale of picoseconds [36–39]. The relevant dimensional features of the titania nanotube arrays, i.e. half the wall thickness, are all smaller than 10 nm which is less than the retrieval length of crystalline titania [40], hence bulk recombination is greatly reduced and the quantum yield enhanced [35,40–42]. We note that van de Lagemaat and co-workers observed a substantial enhancement of the quantum yield in SiC made nanoporous by anodic etching in HF solution [39]. Furthermore charge carriers near the electrolyte–nanotube interface region are readily accessible to the electrolyte species due to overlapping wave functions [36].

4. Conclusions

Our results show that the highly ordered nanotube arrays present an excellent photoelectrochemical material platform architecture that is both low cost (i.e. practical) and stable against photocorrosion with no detectable sample degradation over testing periods of several months. Under AM 1.5 illumination a 6 μm nanotube array annealed at 600 °C generates hydrogen by water photoelectrolysis at a Watt-normalized rate of 1.75 mL/W h. There is no variation in the hydrogen generation rate with time.

There is a distinct dependence of the photoelectrochemical properties on sample annealing, and hence crystallization. The crystallites in the tube walls as well as barrier layer grow on annealing at elevated temperature [20]. The width of the anatase crystallites in the wall is restricted by the wall thickness, however, growth might occur along the length of the tube. Compared to samples annealed at relatively lower temperatures, the nanotube array samples annealed at higher temperatures have less amorphous regions (that provide carrier recombination centers), higher connectivity between grains, and reduced number of grain boundaries due to the consumption of the smaller crystallites by the larger crystallites during grain growth. Further work in planned to be to confirm this, as well as efforts focused on bandgap engineering of the material architecture to maximize its response in the visible light region.

References

[1] A.J. Bard, M.Z. Fox, Artificial photosynthesis: solar splitting of water to hydrogen and oxygen, Acc. Chem. Res. 28 (1995) 141–145.

[2] A. Fujishima, K. Honda, Electrochemical photolysis of water at a semiconductor electron, Nature 238 (1972) 37–41.

[3] J.R. Bolton, Solar photoproduction of hydrogen: a review, Solar Energy 57 (1996) 37–50.

[4] V.M. Aroutiounian, V.M. Arakelyan, G.E. Shahnazaryan, Metal oxide photoelectrodes for hydrogen generation using solar radiation-driven water splitting, Solar Energy 78 (2005) 581–592.

[5] M. Gratzel, Dye-sensitized solar cells, J. Photochem. Photobiol. C: Photochem. Rev. 4 (2003) 145–153.

[6] M. Ashokkumar, An overview on semiconductor particulate systems for photoproduction of hydrogen, Int. J. Hydrogen Energy 23 (1998) 427–438.

[7] M. Gratzel, Photoelectrochemical cells, Nature 414 (2001) 338–344.

[8] M. Gratzel, Conversion of sunlight to electric power by nanocrystalline dye-sensitized solar cells, J. Photochem. Photobiol. A: Chem. 164 (2004) 3–14.

[9] M.K. Nazeeruddin, P. Pechy, T. Renouard, S.M. Zakeeruddin, R. Humphry-Baker, P. Comte, P. Liska, L. Cevey, E. Costa, V. Shklover, L. Spiccia, G.B. Deacon, C.A. Bignozzi, M. Gratzel, Engineering of efficient panchromatic sensitizers for nanocrystalline TiO_2-based solar cells, J. Am. Chem. Soc. 123 (2001) 1613–1624.

[10] F. Cao, G. Oskam, G.J. Meyer, P.C. Searson, Electron transport in porous nanocrystalline TiO_2 photoelectrochemical cells, J. Phys. Chem. 100 (1996) 17021–17027.

[11] P.E. deJongh, D. Vanmaekelbergh, Trap-limited electronic transport in assemblies of nanometer-size TiO_2 particles, Phys. Rev. Lett. 77 (1996) 3427–3430.

[12] X. Zhang, et al., Electrochemical fabrication of single-crystalline anatase TiO_2 nanowire arrays, J. Electrochem. Soc. 148 (2001) G398–G400.

[13] S.J. Limmer, T.P. Chou, G.Z. Cao, A study on the growth of TiO_2 nanorods using sol electrophoresis, J. Mater. Sci. 39 (2004) 895–901.

[14] S. Yoo, S.A. Akbar, K.H. Sandhage, Nanocarving of bulk titania crystals into oriented arrays of single-crystal nanofibers via reaction with hydrogen-bearing gas, Adv. Mater. 16 (2004) 260–263.

[15] M. Adachi, Y. Murata, I. Okada, S. Yoshikawa, Formation of titania nanotubes and applications for dye-sensitized solar cells, J. Electrochem. Soc. 150 (2000) G488–G493.

[16] Y.C. Zhu, H.L. Li, Y. Koltypin, Y.R. Hacohen, A. Gedanken, Sonochemical synthesis of titania whiskers and nanotubes, Chem. Commun. 24 (2001) 2616–2617.

[17] T.Y. Peng, A. Hasegawa, J.R. Qiu, K. Hirao, Fabrication of titania tubules with high surface area and well-developed mesostructural walls by surfactant-mediated templating method, Chem. Mater. 15 (2003) 2011–2016.

[18] I.M. Butterfield, Applied studies on immobilized titanium dioxide films as catalysts for the photoelectrochemical detoxification of water, J. Appl. Electrochem. 27 (1997) 385–395.

[19] D. Gong, C.A. Grimes, O.K. Varghese, W. Hu, R.S. Singh, Z. Chen, E.C. Dickey, Titanium oxide nanotube arrays prepared by anodic oxidation, J. Mater. Res. 16 (2001) 3331–3335.

[20] O.K. Varghese, D.W. Gong, M. Paulose, C.A. Grimes, E.C. Dickey, Crystallization and high-temperature structural stability of titanium oxide nanotube arrays, J. Mater. Res. 18 (2003) 156–165.

[21] G.K. Mor, O.K. Varghese, M. Paulose, N. Mukherjee, C.A. Grimes, Fabrication of tapered, conical-shaped titania nanotubes, J. Mater. Res. 18 (2003) 2588–2593.

[22] G.K. Mor, K. Shankar, O.K. Varghese, C.A. Grimes, Photoelectrochemical properties of titania nanotubes, J. Mater. Res. 19 (2004) 2989–2996.

[23] G.K. Mor, M.A. Carvalho, O.K. Varghese, M.V. Pishko, C.A. Grimes, A room temperature TiO_2-nanotube hydrogen sensor able to self-clean photoactively from environmental contamination, J. Mater. Res. 19 (2004) 628–634.

[24] O.K. Varghese, G.K. Mor, C.A. Grimes, M. Paulose, N. Mukherjee, A titania nanotube-array room-temperature sensor for selective detection of hydrogen at low concentrations, J. Nanosci. Nanotechnol. 4 (2004) 733–737.

[25] Q. Cai, M. Paulose, O.K. Varghese, C.A. Grimes, The effect of electrolyte composition on the fabrication of self-organized titanium oxide nanotube arrays by anodic oxidation, J. Mater. Res. 20 (2005) 230–236.

[26] G.K. Mor, K. Shankar, M. Paulose, O.K. Varghese, C.A. Grimes, Enhanced photocleavage of water using titania nanotube arrays, Nano. Lett. 5 (2005) 191–195.

[27] P.R. Mishra, P.K. Shukla, A.K. Singh, O.N. Srivastava, Investigation and optimization of nanostructured TiO_2 photoelectrode in regard to hydrogen production through photoelectrochemical process, Int. J. Hydrogen Energy 28 (2003) 1089–1094.

[28] K.H. Yoon, D.K. Seo, Y.S. Cho, D.H. Kang, Effect of Pt layers on the photoelectrochemical properties of a WO_3/p-Si electrode, J. Appl. Phys. 84 (1998) 3954–3959.

[29] K.-N.P. Kumar, K. Keizer, A.J. Burggraaf, T. Okubo, H. Nagamoto, Textural evolution and phase transformation in titania membranes. Part 2. Supported membranes, J. Mater. Chem. 3 (1993) 1151–1155.

[30] P.I. Gouma, M.J. Mills, Anatase-to-rutile transformation in titania powders, J. Am. Ceram. Soc. 84 (2001) 619–621.

[31] S.U.M. Khan, M. Al-Shahry, W.B. Ingler Jr., Efficient photochemical water splitting by a chemically modified n-TiO_2, Science 297 (2002) 2243–2245.

[32] F.Y. Oliva, L.B. Avalle, E. Santos, O.R. Camara, Photoelectrochemical characterization of nanocrystalline TiO_2 films on titanium substrates, J. Photochem. Photobiol. A: Chem. 146 (2002) 175–188.

[33] Y.V. Pleskov, M.D. Krotova, Photosplitting of water in a photoelectrolyser with solid polymer electrolyte, Electrochim. Acta 38 (1993) 107–109.

[34] D. Vanmaekelbergh, P.E. de Jongh, Driving force for electron transport in porous nanostructured photoelectrodes, J. Phys. Chem. B 103 (1999) 747–750.

[35] A. Hamnett, Porous-electrodes for water oxidation, Faraday Discuss. Chem. Soc. 70 (1980) 127–134.

[36] A. Hagfeldt, M. Gratzel, Light-induced redox reactions in nanocrystalline systems, Chem. Rev. 95 (1995) 49–54.

[37] J.P.H. Sukamto, C.S. Mcmillan, W. Smyrl, Photoelectrochemical investigations of thin metal-oxide films—TiO_2, Al_2O_3, and HFO_2 on the parent metals, Electrochim. Acta 38 (1993) 15–27.

[38] J.P.H. Sukamto, W.H. Smyrl, C.S. Mcmillan, M.R. Kozlowski, Photoelectrochemical measurements of thin oxide-films—multiple internal-reflection effects, J. Electrochem. Soc. 139 (1992) 1033–1043.

[39] J. van de Lagemaat, M. Plakman, D. Vanmaekelbergh, J.J. Kelly, Enhancement of the light-to-current conversion efficiency in an n-SiC/solution diode by porous etching, Appl. Phys. Lett. 69 (1996) 2246–2248.

[40] W.H. Lubberhuizen, D. Vanmaekelbergh, E. Van Faassen, Recombination of photogenerated charge carriers in nanoporous gallium phosphide, J. Porous Mater. 7 (2000) 147–152.

[41] N. Kopidakis, K. Benkstein, J. van de Lagemaat, A.J. Frank, Transport-limited recombination of photocarriers in dye-sensitized nanocrystalline TiO_2 solar cells, J. Phys. Chem. B 107 (2003) 11307–11315.

[42] K.D. Benkstein, N. Kopidakis, J. van de Lagemaat, A.J. Frank, Influence of the percolation network geometry on electron transport in dye-sensitized titanium dioxide solar cells, J. Phys. Chem. B 107 (2003) 7759–7767.